International Journal of Innovative Computing, Information and Control
Volume **8**, Number **5(B)**, May **2012**

ICIC International ©2012 ISSN 1349-4198
pp. 3553–3563

A NOVEL ADAPTIVE LEAK DIAGNOSIS AND LOCALIZATION METHOD FOR INFRARED IMAGE

Ling Zhao[1], Tao Wang[1], Peng Shi[2,3] and Meiling Wang[1]

[1]School of Automation
Beijing Institute of Technology
No. 5, South Zhongguancun Street, Haidian District, Beijing 100081, P. R. China
zhaoling84@gmail.com; {wangtaobit; wangml}@bit.edu.cn

[2]College of Information Engineering
Northwest A&F University
Yangling, Shaanxi, 712100, China

[3]School of Engineering and Science
Victoria University
PO Box 14428, Melbourne, VIC 8001, Australia
peng.shi@vu.edu.au

Received February 2011; revised June 2011

Abstract. *In this paper, a new adaptive diagnosis and localization method is given for small target leak points in an infrared image. The infrared image of a test vessel with cold compressed air is photographed by a thermal camera. Based on a mathematical model of the infrared image, the diagnosis and localization method is given as an adaptive algorithm which is synthesized by a developed adaptive center-weighted median filter and an improved adaptive kernel regression method. Experimental results are given to illustrate the proposed algorithm is effective and adaptable to small target detection under the complex infrared image background.*
Keywords: Leak diagnosis and localization, Kernel regression, Infrared image, Spatially adaptive

1. **Introduction.** In the nearly decades, detection and localization in air-leakage test are much important for many manufacturing processes. With the development of technology, more and more requirements are needed to meet for detection and localization of leak points. Generally, there are three traditional ways to find tiny leak points in vessels: air bubbling test, mass spectrometry and ultrasonic positioning. However, the three traditional ways cannot simultaneously overcome the disadvantages of low efficiency and poor anti-jamming ability [1, 2]. With the development of infrared technology, infrared thermography has been used in the field of defect diagnosis and detection in recent years, for example, [3, 4, 5, 6] and the references therein. The random noise in infrared images with distinguishing small targets has to be further handled by a suitable filter method. An approach to fast noise reduction of infrared images has been given in [7]. It is known that adaptive filter method has been widely used to deal with random noise, such as in [8, 9, 10, 11]. A non-uniformity correction algorithm based on adaptive filter for infrared focal plane arrays has been given in [13]. An adaptive image enhancement approach to infrared images for long-range surveillance has been presented in [14]. An adaptive center weighted median filter has been proposed for improving the performance of median-based filters and preserving image details while effectively suppressing impulsive noise in [20].

The leak detection has developed many years. However, to the best of our knowledge, there have been few results on infrared applied in the field of leak detection for tank. In this paper, we firstly introduce infrared image in this field of Leak detection. A computer-based system that combines a specific pneumatic circuit with an on-line infrared camera is proposed to determine the air-tightness of a test vessel. In the computer-based system, the test object is charged with cryogenic compressed air, and its temperature field is acquired by infrared thermography. The leakage points can be identified by means of the designed adaptive diagnosis and localization algorithm on the basis of the infrared image. Furthermore, this adaptive method can improve the detection efficiency of the actual production and reduce the workload in factory. Selecting the most appropriate algorithms for detecting small targets in infrared image scenes is necessary, since the characteristics between small targets and backgrounds are difficult to distinguish. To solve the problem, a criterion has been proposed to measure the difficulty in distinguishing small targets from infrared images [12]. A kernel-based nonparametric regression method for clutter removal in infrared small-target detection applications has been given in [15]. Based on Taylor expansion, an improved kernel regression method has been presented in [16]. The kernel regression has also been extended by an adaptive method for debluring applications in [17]. Up to now, there have been few results developed for the purpose of detecting small targets in varied infrared image scenes by using an adaptive kernel regression method. This problem, which motivates us to make the effort, is important and challenging in both theory and industry.

In this paper, we propose the adaptive diagnosis and localization method for detecting small targets in varied infrared image scenes. Both the adaptive center-weighted median filter and the adaptive kernel regression method are developed to the synthesize adaptive algorithm. Some experimental results are also given to illustrate the effectiveness of the algorithm. The paper is organized as follows. In Section 2, the model of infrared image is described. Section 3 gives the developed adaptive center-weighted median filter and the improved adaptive kernel regression method. The synthesize adaptive algorithm is also given in this section. In Section 4, we present an application of the adaptive synthesize algorithm in an experiment. Conclusions are given in Section 5.

2. **Problem Statement and Preliminaries.**

2.1. **Experimental model of leak diagnosis and localization.**

To improve the detection efficiency for the vessel, a novel leak diagnosis and localization model is introduced based on infrared thermography and image processing. The leak diagnosis and localization model used in the experiment is shown in Figure 1.

As is shown in Figure 1, a thermal camera is used as the infrared acquisition device for its strong on-line capture features. A RGB infrared image photographed by the thermal camera with temperature change is obtained in real time during the experiment. Because of the double influences of Joule-Thomson and heat transfer effects generated by leakage flow, the temperature field around a leak point is shown as singular pixels in the RGB infrared image. The RGB infrared image will be sent to a computer for the further processing to locate the leak points by using the designed adaptive diagnosis and localization algorithm in this paper.

The diagram of pneumatic circuitry term of Figure 1 in the experiment is shown in Figure 2.

It is seen from Figure 2 that from left to right there are several components: air source, auxiliary components, precision regulator, magnetic valve, active cooler, pressure sensor, test vessel, thermal camera, and so on. The pipelines between the active cooler and

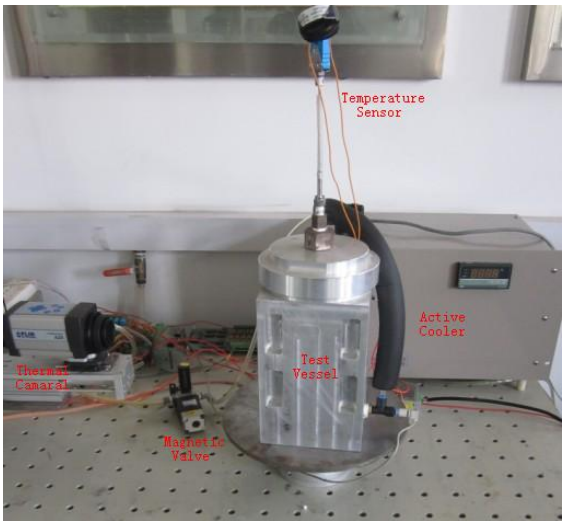

FIGURE 1. Leak diagnosis and localization apparatus

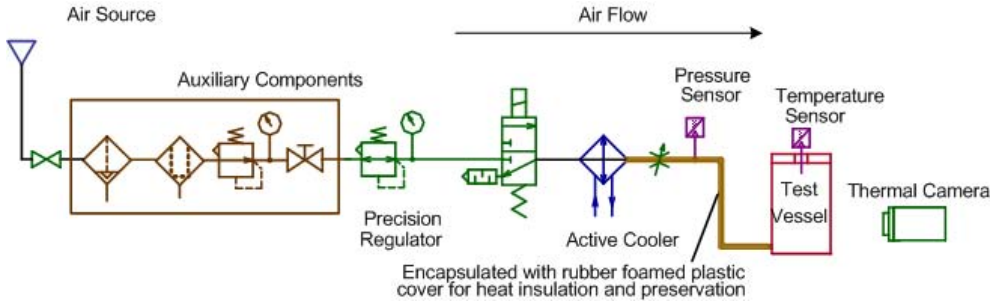

FIGURE 2. The diagram of pneumatic control system

the test vessel are encapsulated with rubber foamed plastic cover for heat insulation and preservation.

2.2. **Mathematical model of the infrared image.** Since the red component and blue component have no relation with the leak point in the RGB infrared image, they are ignored in the following image process. Extracting the green component of the RGB infrared image with leak points, we obtain a gray image which is used as the original image. The original infrared image with small target leak points during the experiment consists of three components: target points, background, and noise. Let

$$K = \{(x, y)|1 \leq x \leq V, 1 \leq y \leq W\}$$

denote the pixel coordinates of the original infrared image, where V and W are two integral numbers which denote the height and width, respectively. The original infrared image can be described by the following functional model:

$$f(x, y) = f_T(x, y) + f_B(x, y) + n(x, y) \tag{1}$$

where $f(x, y)$ is the gray scale of a pixel (x, y) at the original infrared image, $f_T(x, y)$ is the gray scale of a pixel at the region of targets, $f_B(x, y)$ is the gray scale of a pixel at the background, and $n(x, y)$ is the intensity of the random noise. In the following section, an adaptive center-weighted median filter is developed to deal with the random noise $n(x, y)$. Then, an adaptive kernel regression method of target detection is improved to eliminate the background component $f_B(x, y)$. In the end, a synthesize adaptive diagnosis

and localization algorithm is given for the small region of leak targets $f_T(x, y)$ based on the infrared image model (1).

3. Main Results.

3.1. **Adaptive center-weighted median filter.** Let $x(k)$ represent the input pixel value of the original infrared image at location $k \in K$. At each location k, the adaptive filter window $w\{k\}$ in terms of the coordinates symmetrically surrounding the input pixel $x(k)$ is defined as follows:

$$w\{k\} = \{x_f(k) | f = 1, 2, \cdots, n, n+1, \cdots, N\}$$

where $N = 2n + 1$ with n is a non-negative integer. Therefore, the input center pixel of the adaptive center-weighted median filter is $x(k) = x_{n+1}(k)$. The output of adaptive center-weighted median filter is

$$y(k) = y_c(k) = \mathbf{MED}(w_c\{k\}),\ c = 0, 1, \cdots, N$$

where **MED** denotes the median operation and

$$w_c\{k\} = \{x_1(k), \cdots, x_n(k), c \diamond x_{n+1}(k), x_{n+2}(k), \cdots, x_N(k)\}$$

where

$$c \diamond x_{n+1}(k) = \underbrace{x_{n+1}(k) + \cdots + x_{n+1}(k)}_{c}$$

in which $\diamond$ represents the repetition operation and c denotes the number of $x_{n+1}(k)$. The $\mathbf{MED}(w_c\{k\})$ outputs the $(N+c)/2$th largest value of the filter window $w_c\{k\}$. Therefore, the key term of the adaptive center-weighted median filter is how to obtain the adaptive center weight c.

Let $O(k)$ be the observation vector of the adaptive center-weighted median filter. To generate the observation vector $O(k)$, the following two variables are given as:

$$u(k) = |x(k) - \mathbf{MED}(w\{k\})| \tag{2}$$

$$v(k) = \frac{|x(k) - x_{c1}(k)| + |x(k) - x_{c2}(k)|}{2} \tag{3}$$

where

$$|x(k) - x_{c1}(k)| \le |x(k) - x_{c2}(k)| \le |x(k) - x_i(k)|,\ 1 \le i \le 2n + 1,$$

and i is not equal to $n + 1$, $c1$ or $c2$. $u(k)$ denotes the absolute difference between the input $x(k)$ and the median value of $w\{k\}$. Note that the values of $x_{c1}(k)$ and $x_{c2}(k)$ are selected to be the two closest values of $x(k)$ in the filter window $w\{k\}$. If only $u(k)$ is considered, line component in $w\{k\}$ will be identified as noise. Hence, we also apply the variable $v(k)$ such that the input $x(k)$ will not be identified as noise for the reason of that the variable $v(k)$ is small enough.

By using the two inequalities (2) and (3), the observation vector $O(k)$ can be calculated as

$$O(k) = (u(k), v(k)) \in R^2$$

It is determined that the R^2 observation vector space is partitioned into M mutually exclusive blocks

$$\{\Omega_i,\ i = 1, 2, \cdots, M\}$$

with

$$\Omega_i = \left\{O(k) \in R^2 :\ f(O(k)) = i\ \right\},\ i = 1, 2, \cdots, M$$

where the classifier $f(\cdot)$ is defined as a function of the observation vector $O(k)$. That is, it determines the partitioning of the observation vector space R^2 into M non-overlapping blocks according to the value of the observation vector $O(k) \in R^2$. Hence, we have

$$R^2 = \bigcup_{i=1}^{M} \Omega_i, \ i = 1, 2, \cdots, M$$

and

$$\Omega_i \cap \Omega_j = \phi, \ \forall \ i \neq j, \quad i, j = 1, 2, \cdots, M$$

Each input data $x(k)$ corresponding to its observation vector $O(k)$ is only classified into one of those M blocks according to the classifier $f(\cdot)$. The classifier $f(\cdot)$ can be designed by using a simple scalar quantization since the partitioning indices are decided with low computational complexity in the training and filtering process [18].

It is decided that $u(k)$ belongs to an interval Ω_j with $j = 1, 2, \cdots, M$ and $v(k)$ belongs to an interval Ω_l with $l = 1, 2, \cdots, M$, respectively. Evaluate $O(k)$ that belongs to block i of the partition such that $O(k) \in \Omega_i$, $i \in \{1, 2, \cdots, M\}$ by using the equation $i = (j-1) \cdot B + l$ where B denotes the number of intervals of $u(k)$ and $v(k)$. When we obtain the expected value $f(O(k)) = i$, the conditional mean square error is shown as

$$\hat{\epsilon}_i(k) = E[e^2(k)|f(O(k)) = i] = E[(d(k) - y(k))^2|f(O(k)) = i]$$

where $E[\cdot|\cdot]$ is the conditional expectation, the error $e(k)$ is the difference between the desired output $d(k)$ and the physical output $y(k)$. Because the M blocks are mutually exclusive, the total minimum mean square error ϵ is expressed as

$$\epsilon = \sum_{i=1}^{M} [\hat{\epsilon}_i(k)|f(O(k)) = i]$$

In the following, we design the optimal weight $\alpha_i(k)$ with $i = 1, 2, \cdots, M$ by using the least mean square algorithm which is capable of minimizing the error function $\epsilon_i(k)$ with respect to the block Ω_i as in [19]. The iterative learning algorithm of $\alpha_i(k)$ is derived as

$$\alpha_i^{t+1}(k) = \begin{cases} \alpha_i^t(k) - \eta_i |e(k)||x(k) - d(k)|, & \alpha_i^{t+1}(k) \geq 0, \\ 0, & \alpha_i^{t+1}(k) < 0. \end{cases}$$

where η_i denotes a learning rate, $\alpha_i^0(k)$ denotes the initial weight and $\alpha_i^t(k)$ denotes the weight after the tth iteration, $t = 0, 1, \cdots$. Furthermore, every weight within block Ω_i is initialized with N. That is, the weights are set such that

$$\alpha_i^0(k) = N, \ i = 1, 2, \cdots, M,$$

based on which the output of the adaptive center-weighted median filter is equal to the input pixel $x(k)$ since the center weight $\alpha_i^0(k)$ is N. Moreover, the filter will degenerate into a standard median filter when the weight $\alpha_i^0(k)$ decreases from N to 1. For the derivation of least mean-squares (LMS) convergence, the following conditions are sufficient for the convergence in the mean and mean square:

$$0 < \eta_i < \frac{2}{E[(d(k) - y(k))^2|f(O(k)) = i]}, \ i = 1, 2, \cdots, M$$

It is obtained that $\alpha_i(k)$ with $i = 1, 2, \cdots, M$ serves as the adaptive weight c for the adaptive center-weighted median filter as in [20].

By using the adaptive center-weighted median filter, the noise term $n(x, y)$ in model (1) is eliminated. That is, the infrared image model (1) can be changed to

$$f(x, y) = f_T(x, y) + f_B(x, y) \tag{4}$$

after the filter manipulate.

3.2. **Adaptive kernel regression method.** The nonparametric statistical regression model of 2-D sample data is written as follows:

$$g_i = m(z_i) + \varepsilon_i,\ z_i = [x_i, y_i],\ i = 1, 2, \cdots, N$$

where g_i is the image gray of a sample pixel, (x_i, y_i) is the spatial coordinates of a sample pixel, $m(z_i)$ is the regression function whose form is unspecified, which should be a nonlinear function to approximate the complex background better, ε_i is a random error or interference that is uncorrelated with $m(z_i)$, N is the total number of sample pixels which are used to estimate the regression model. In this paper, ε_i is supposed to be a Gaussian random variable with zero mean.

Under the complex background, the parametric regression model for estimation is adaptive. Considering the complexity of background fluctuation, nonparametric regression is more reasonable in fitting the background component. To estimate the value of regression function at any point z, if z is near the sample z_i, the local expansion of the regression function $m(z_i)$ can be utilized. Therefore, the local signal representation of the unknown function with a Taylor series is

$$m(z_i) = m(z) + \{\nabla m(z)\}^T (z_i - z) + \frac{1}{2}(z_i - z)^T \{\mathbf{H} m(z)\}(z_i - z) + \cdots \tag{5}$$

where ∇ is the gradient (2×1) operator and $\mathbf{H}$ is the Hessian (2×2) operator, which is a symmetrical matrix. Moreover, it is obtained that (5) can be rewritten as follows:

$$m(z_i) = \beta_0 + \beta_1^T (z_i - z) + \beta_2^T vech\{(z_i - z)(z_i - z)^T\} + \cdots \tag{6}$$

where $vech(\cdot)$ is the half-vectorization operator which lexicographically orders the lower triangular portion of a symmetric matrix into a column-stacked vector, e.g.,

$$vech\left\{\begin{bmatrix} a & b \\ b & c \end{bmatrix}\right\} = \begin{bmatrix} a & b & c \end{bmatrix}$$

$$vech\left\{\begin{bmatrix} a & b & c \\ b & d & e \\ c & e & f \end{bmatrix}\right\} = \begin{bmatrix} a & b & c & d & e & f \end{bmatrix}$$

Furthermore, β_0 is $m(z)$, which is the pixel value of interest, and the vectors β_1 and β_2 are

$$\beta_1 = \begin{bmatrix} \dfrac{\partial m(z)}{\partial x} & \dfrac{\partial m(z)}{\partial y} \end{bmatrix}^T$$

$$\beta_2 = \begin{bmatrix} \dfrac{\partial^2 m(z)}{2\partial x^2} & \dfrac{\partial^2 m(z)}{\partial x \partial y} & \dfrac{\partial^2 m(z)}{2\partial y^2} \end{bmatrix}^T$$

A logical step to take is to estimate the parameters β_j from all the samples $\{g_i\}_{i=1}^N$, while giving the nearby samples higher weights than samples farther away. A formulation of the fitting problem capturing this idea is to solve the following optimization problem:

$$\min_{\beta_j} \sum_{i=1}^{N} \left[g_i - \beta_0 - \beta_1^T (z_i - z) - B_2 - \cdots\right]^2 \cdot \mathcal{K}_{adapt}(z_i - z, g_i - g) \tag{7}$$

with

$$B_2 = \beta_2^T vech\{(z_i - z)(z_i - z)^T\}$$

where $\mathcal{K}_{adapt}$ is an adaptive kernel function which rely on not only the spatial distances $(z_i - z)$ but also on the gray distances $(g_i - g)$. Based on the data-adapted steering kernel in [17], we take the adapted kernel $\mathcal{K}_{adapt}$ in this paper as the following form

$$\mathcal{K}_{adapt}(z_i - z, g_i - g) = \mathcal{K}_{\mathbf{H}_i^s}(z_i - z)$$

where $\mathbf{H}_i^s$ are now data-adaptive full (2×2) steering matrices which are defined as

$$\mathbf{H}_i^s = h\mu C_i^{-\frac{1}{2}}$$

where h is the global smoothing parameter, μ is a scalar capturing local density of samples and it is nominally set to one, C_i are symmetric inverse covariance matrices based on differences in the local gray-values. The local edge structure is related to the gradient covariance, where a naive estimate of this covariance matrix may be obtained as follows:

$$\hat{C}_i \approx \begin{bmatrix} \sum m_{z_1}(z_j) m_{z_1}(z_j) & \sum m_{z_1}(z_j) m_{z_2}(z_j) \\ \sum m_{z_2}(z_j) m_{z_1}(z_j) & \sum m_{z_2}(z_j) m_{z_2}(z_j) \end{bmatrix}, \; z_j \in \xi_i$$

where ξ_i is a local analysis window around the position of interest, $m_{z_1}(\cdot)$ and $m_{z_2}(\cdot)$ are the first derivatives along and axes, respectively. In order to have a stable estimation for the covariance matrix, we parameterize and regularize it as follows:

$$C_i = \gamma_i \mathcal{R}_{\theta_i} \Lambda_i \mathcal{R}_{\theta_i^T}$$

with

$$\mathcal{R}_{\theta_i} = \begin{bmatrix} \cos(\theta_i) & \sin(\theta_i) \\ -\sin(\theta_i) & \cos(\theta_i) \end{bmatrix}, \; \Lambda_i = \begin{bmatrix} \sigma_i & 0 \\ 0 & \sigma_i^{-1} \end{bmatrix}$$

where $\mathcal{R}_{\theta_i}$ is a rotation matrix and Λ_i is an elongation matrix. Now the covariance matrix C_i is given by the three parameters γ_i, θ_i and σ_i, which are the scaling, rotation and elongation parameters, respectively.

The optimization problem (7) can be described as a weighted least-square estimation model. That is, we only calculate β_0 from the estimation model for the reason of that the gray scale of the pixels is the key point to focus on. The matrix form of the estimation model is written as follows:

$$\hat{m}(z) = \hat{\beta}_0 = \mathbf{e}_1^T (\mathbf{Z}_z^T \mathbf{W}_z \mathbf{Z}_z) \mathbf{Z}_z^T \mathbf{W}_z \mathbf{g} \tag{8}$$

where

$$\mathbf{e}_1 = [1, 0, 0, \cdots]^T, \; \mathbf{g} = [g_1, g_2, \cdots, g_N]^T$$

$$\mathbf{W}_z = diag\{\mathcal{K}_{adapt}(z_1 - z), \mathcal{K}_{adapt}(z_2 - z), \cdots, \mathcal{K}_{adapt}(z_N - z)\}$$

$$\mathbf{Z}_z = \begin{bmatrix} 1 & (z_1 - z)^T & vech\{(z_i - z)(z_i - z)^T\} & \cdots \\ 1 & (z_1 - z)^T & vech\{(z_i - z)(z_i - z)^T\} & \cdots \\ \vdots & \vdots & \vdots & \vdots \\ 1 & (z_1 - z)^T & vech\{(z_i - z)(z_i - z)^T\} & \cdots \end{bmatrix}$$

The proposed method is based on background prediction with the purpose of obtaining an exact estimation of the background clutter $\hat{f}_B(x, y)$. After the aforementioned matrix operation, the value of gray at any pixel can be estimated precisely from the statistical regression model, and the prediction of the entire image can be obtained. It is easy to show that (4) can be written as

$$f(x, y) = f_T(x, y) + \hat{f}_B(x, y) + \varepsilon \tag{9}$$

where ε is the bias of the kernel regression prediction. Letting $\hat{f}_B(x,y) = \hat{m}(z)$ according to (8), the "pure" target-like infrared image model is represented as follows

$$f(x,y) = f_T(x,y) + \varepsilon \tag{10}$$

3.3. **Adaptive diagnosis and localization algorithm.** The steps of the synthesize adaptive diagnosis and localization algorithm for small target leak points in infrared image are given as follows.

1. Extract the green component of the RGB infrared image with leak point as the original infrared image modeled as (1).
2. By using the obtained adaptive center-weighted median filter, the noise $n(x,y)$ in (1) is eliminated. The original infrared image model is changed to (4).
3. The histogram equalization method is used to enhance the brightness and contrast degree of the infrared image gotten from step 2.
4. Predict the background clutter of the image obtained from step 3 by the adaptive kernel regression method in this paper. The predicted background clutter is eliminated from the original image to obtain the target-like image include potential target points term $f_T(x,y)$ and the bias of kernel regression prediction ε as (10).
5. Extract the leak point from the target-like image by simple threshold segmentation method, the bias of kernel regression prediction ε is omitted and the target points term $f_T(x,y)$ is obtained.
6. Mark out the leak point by small rectangle in the original image.

4. **Experimental Results.** The tested side of the vessel in our experiment is given in the following figure:

FIGURE 3. The tested side of the vessel

In this experiment, we just randomly choose one of the small target leak points in the tested side of the vessel as diagnosis target which has been remarked by a red rectangle "□" in Figure 3. The experiments are done under the following conditions:

The FLIR A20m thermal camera is chosen in the experiment
The cast aluminum test vessel contained 500mL of air
The flow rate of the leak is 85mL/min
The inflation pressure is 0.6MPa
The temperature of the compressed air in active cooler is 254K
The ambient temperature is 286K

By using the above conditions, we get one of the RGB infrared image which is sent to a computer for the processing of extracting the green component of the RGB infrared

image with leak points. In Figure 4, image (a) is the chosen RGB infrared image which shows the temperature field of the vessel before inflation, image (b) is the gray original image gotten from the green component of image (a).

(a) RGB image (b) Original image

FIGURE 4. The images before inflation

Another RGB infrared image after inflation of the cold compressed air is obtained and sent to a computer for the processing to locate the leak point in Figure 3. Utilizing the adaptive diagnosis and localization algorithm, a series of images are obtained during the image process. All the images are shown in Figure 5. The test vessel is inflated by cold compressed air, its temperature field especially around leak the point changes a lot. It is obviously shown by comparing the difference between Figure 4 and the two images (a) and (b) in Figure 5.

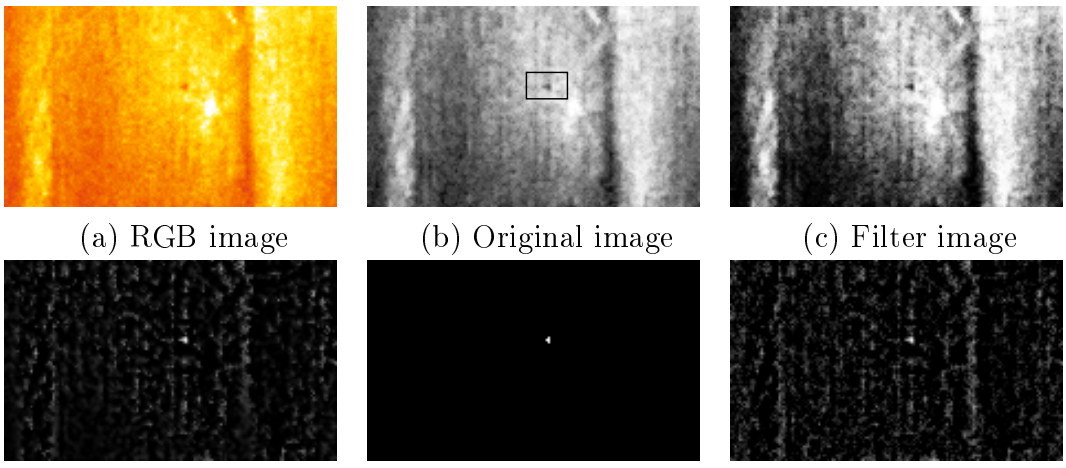

(a) RGB image (b) Original image (c) Filter image

(d) Target image (e) Result image (f) Compare image

FIGURE 5. The images after inflation

Figure 5(a) is the chosen RGB infrared image which shows the temperature field of the vessel at 100s after inflation.

Figure 5(b) is the gray original image gotten from the green component of the RGB infrared image (a) after step 1 of the algorithm.

Figure 5(c) is the filter image after step 2 and step 3 of the algorithm. It is obtained from the result of using adaptive center-weighted median filter and histogram equalization method to image (b).

Figure 5(d) is the target-like image without background clutter after step 4 of the algorithm. It is obtained from the result of using adaptive kernel regression method to image (c).

Figure 5(e) is the detected result image of the test after step 5 of the algorithm. The white point is the leak point that we want to find. The leak point is marked out by the rectangle "□" in image (b) after step 6 of the algorithm.

Figure 5(f) is also a target-like image by using the kernel regression method in [15].

The same initial parameters are used for images (d) and (f) in Figure 5, respectively. Letting

$$m_{\max} = \max\{m(x,y) | 1 \le x \le V, 1 \le y \le W\},$$

the peak signal to noise ratio (PSNR) is defined as follows:

$$\mathrm{PSNR} = 10 \lg \left[\frac{m_{\max}^2}{\frac{1}{(V+1)(W+1)} \sum_{x=1}^{V} \sum_{y=1}^{W} |m(x,y) - \hat{m}(x,y)|} \right]$$

Then, we have that

$$\mathrm{PSNR}(d) = 21.3, \ \mathrm{PSNR}(f) = 17.6,$$

where $\mathrm{PSNR}(d)$ and $\mathrm{PSNR}(f)$ denote the PSNR of (d) and (f), respectively.

Remark 4.1. *The leak detection has developed many years. However, to the best of our knowledge, there have been few results on infrared applied in the field of leak detection for tank. Leak detection based on infrared image is firstly introduced in this field in the paper. Compared with the former three traditional ways, the designed adaptive diagnosis and localization algorithm can improve the detection efficiency of the actual production and reduce the workload in factory.*

Remark 4.2. *In the experimental results, we have the leak point is much more distinct in image (e) than image (f) in Figure 5. Furthermore, from the inequality* $21.3 > 17.6$ *which means* $PSNR(d) > PSNR(f)$*, it is illustrated that we have obtained a better peak signal to noise ratio by using the adaptive diagnosis and localization algorithm than the algorithm in* [15]*. Hence, the method used in this paper is better than that of* [15] *in the leak diagnosis and localization system.*

5. **Conclusions.** In this paper, a new adaptive leak diagnosis and localization method has been given for small target points in a infrared image. Both the adaptive center-weighted median filter and the adaptive kernel regression method have been developed in this paper. By using the two developed techniques, an adaptive diagnosis and localization algorithm has been proposed. Through some experimental results, it has been shown that the proposed method generalized previous results available and adaptable to small-target detection under a complex infrared image background.

Acknowledgments. This work was supported by the National Natural Science Foundation of China under Grant(50975025, 60804011, 60904001). This work was also partially supported by the Education Ministry Key Laboratory of Complex System Intelligent Control and Decision Foundation of China , and the Engineering and Physical Sciences Research Council, UK (EP/F029195).

REFERENCES

[1] S. H. Yonak and D. R. Dowling, Parametric dependencies for photoacoustic leak localization, *Journal of the Acoustical Society of America*, vol.112, pp.145-155, 2002.

[2] G. Hessel, Acoustic leak monitoring with neural networks at complicated structures, *Proc. of the 7th International Symposium on Nuclear Reactor Surveillance and Diagnostics*, Avignon, France, vol.11, pp.1-8, 1995.

[3] L. Zhou and Y. Zeng, Automatic alignment of infrared video frames for equipment leak detection, *Analytica Chimica Acta*, vol.584, pp.223-227, 2007.

[4] T. Inagaki, Diagnosis of the leak point on a structure surface using infrared thermography in near ambient conditions, *NDT & E International*, vol.30, pp.135-142, 1997.

[5] T. T. Zin, H. Takahashi and H. Hama, Robust person detection in far infrared images-methods based on multi-slits and GC movement patterns, *International Journal of Innovative Computing, Information and Control*, vol.5, no.3, pp.751-761, 2009.
[6] S.-Y. Cho, C. W. Ting and C. Quek, Thermal facial pattern recognition for personal verification using fuzzy CMAC model, *International Journal of Innovative Computing, Information and Control*, vol.7, no.1, pp.203-222, 2011.
[7] C. Lin, C. Kuo, C. Lai, M. Tsai, Y. Chang and H. Cheng, An approach to fast noise reduction of infrared image, *Infrared Physics & Technology*, vol.54, no.1, pp.1-9, 2011.
[8] H. Masuike and A. Ikuta, Fuzzy adaptive filter for state estimation of sound environment system and its application to psychological evaluation, *International Journal of Innovative Computing, Information and Control*, vol.5, no.12(B), pp.4797-4807, 2009.
[9] Y. Zhu, B. Chen and J. Hu, Adaptive filtering with adaptive p-power error criterion, *International Journal of Innovative Computing, Information and Control*, vol.7, no.4, pp.1725-1738, 2011.
[10] B. Jiang, K. Zhang and P. Shi, Less conservative criteria for fault accommodation of time-varying delay systems using adaptive fault diagnosis observer, *International Journal of Adaptive Control and Signal Processing*, vol.24, no.4, pp.322-334, 2010.
[11] J. Wang, B. Jiang and P. Shi, Adaptive observer based fault diagnosis for satellite attitude control systems, *International Journal of Innovative Computing, Information and Control*, vol.4, no.8, pp.1921-1929, 2008.
[12] K. Huang and X. Mao, Detectability of infrared small targets, *Infrared Physics & Technology*, vol.53, no.3, pp.208-217, 2010.
[13] H. Zhou, H. Qin, R. Lai, B. Wang and L. Bai, Nonuniformity correction algorithm based on adaptive filter for infrared focal plane arrays, *Infrared Physics & Technology*, vol.53, no.4, pp.295-299, 2010.
[14] C.-L. Lin, An approach to adaptive infrared image enhancement for long-range surveillance, *Infrared Physics & Technology*, vol.54, no.2, pp.84-91, 2011.
[15] Y. Gu, C. Wang, B. Liu and Y. Zhang, A kernel-based nonparametric regression method for clutter removal in infrared small-target detection applications, *IEEE Geoscience and Remote Sensing Letters*, vol.7, no.3, pp.469-473, 2010.
[16] J. Zhang, X. Huang and C. Zhou, An improved kernel regression method based on Taylor expansion, *Applied Mathematics and Computation*, vol.193, no.2, pp.419-429, 2007.
[17] H. Takeda, S. Farsiu and P. Milanfar, Deblurring using regularized locally adaptive kernel regression, *IEEE Transactions on Image Processing*, vol.17, no.4, pp.550-563, 2008.
[18] K. Sayood, *Introduction to Data Compression*, 2nd Edition, Morgan Kaufman, 2000.
[19] S. Haykin, *Neural Networks: A Comprehensive Foundation*, 2nd Edition, Prentice-Hall, 1999.
[20] T.-C. Lin, A new adaptive center weighted median filter for suppressing impulsive noise in images, *Information Sciences*, vol.177, no.4, pp.1073-1087, 2007.